# Measurements of the Divergence of Fast Electrons in Laser-Irradiated Spherical Targets

Fast electrons produced by the two-plasmon–decay (TPD) instability[1–4] in direct-drive fusion can deposit their energy into the nuclear fuel (preheat), leading to a reduction in the maximum compression and target performance.[5–8] Typical direct-drive–ignition designs can withstand of the order of ~0.1% of the laser energy converted to preheat[6] before significant degradation occurs. In recent experiments (both planar[9,10] and spherical[11,12]), a Mo layer was used to determine the energy in fast electrons as a fraction of laser energy, using the Mo–$K_\alpha$ line. The energy in fast electrons was found to increase rapidly with laser intensity. At the maximum laser irradiance for spherical targets of ~$1.1 \times 10^{15}$ W/cm$^2$, the energy in fast electrons was ~1% of the laser energy. This is about 10× higher than the maximum that can be tolerated for ignition, and if effectively coupled to the fuel, the effects would be prohibitive. The fast-electron divergence established in this experiment, however, limits the fraction of fast electrons that contribute to preheat. The electrons in the recent experiments were nearly completely absorbed by the Mo layer, providing a measure of the total energy in fast electrons. However, in typical cryogenic direct-drive experiments,[13] the fraction of the fast-electron energy deposited as preheat can be significantly less; only preheat of the compressed fuel shell can be detrimental to target performance. Fast electrons are generated near the end of the laser pulse[4] when the density scale length reaches a maximum. At that time the compressed fuel shell has converged to about half the original target size.[13] Fast electrons produced by TPD are generated near the quarter-critical density layer, and if they have a wide angular divergence, only ~1/4 of the fast electrons will be intercepted by the compressed fuel.
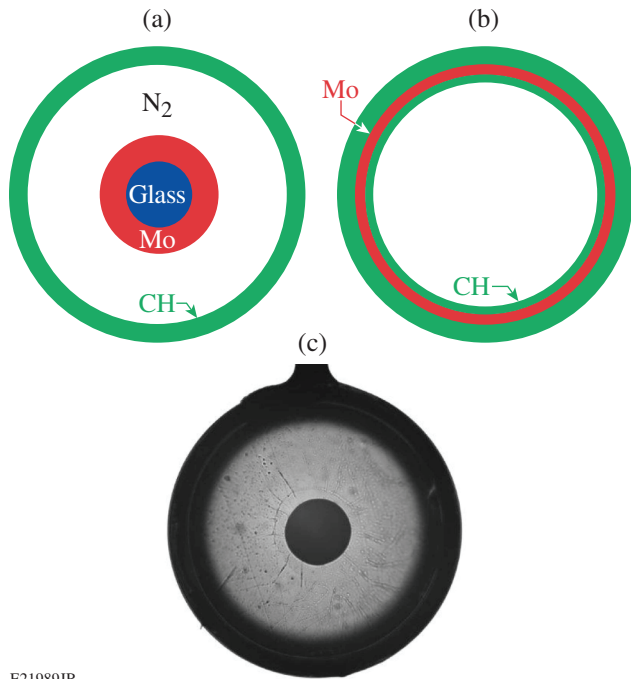
Knowledge of the fast-electron divergence is crucial in assessing their effect on direct-drive experiments and ignition designs. The total energy in fast electrons (as well as the fast-electron temperature) in fusion target implosions is studied using the emitted hard x rays (HXR's).[7,14–16] Without a knowledge of the divergence, the preheat in the compressed fuel cannot readily be determined. This is because the relationship between the measured HXR and the number of fast electrons depends on the atomic number $Z$; therefore (in D$_2$- or DT-filled CH shells) this relationship depends on the partition of the HXR produced by the nuclear fuel and by the outer CH layer. This partition depends on the divergence of fast electrons: the higher the divergence, the larger the fraction of the HXR coming from the CH (since more electrons miss the central fuel shell and travel within the CH). Therefore, an understanding of the fast-electron divergence in laser-fusion experiments is critical for (a) determining the total number of fast electrons, and (b) determining the fraction of the total that is absorbed in the compressed fuel shell.

The fraction 1/4 stated above stems from the fact[13] that at the time of peak fast-electron production, most of HXR-emitting CH mass is comprised within the original target volume. Therefore the relevant fraction of fast electrons is stated with respect to the total number of fast electrons intercepted by the area of the original target surface. Electrons outside this solid angle are not detected and are of no interest.

The divergence of fast electrons was studied with targets [Fig. 135.22(a)] in which Mo-coated solid glass spheres were placed at the center of nitrogen-filled CH shells. A series of targets were irradiated with a 1-ns square pulse while varying the Mo outer diameter $D$ (~200 to 600 $\mu$m). The Mo–$K_\alpha$ line as well as the HXR were measured; both are signatures of fast electrons.[9] To extend the measurements to larger-diameter Mo shells (~800 $\mu$m), a Mo-coated CH shell target overcoated with CH was used [Fig. 135.22(b)]. Figure 135.22(c) is a photograph of the target type illustrated in Fig. 135.22(a), before being shot.

To ensure the same production of fast electrons in all the shots, the outer target diameter was the same (860±1% $\mu$m), as was the laser energy (26 kJ, to within ±1%). To minimize target motion, the outer CH thickness was 50 $\mu$m. This maintained similar underdense hydrodynamic conditions by ensuring a reproducible hot-electron source and limiting instabilities that could result from the acceleration of the shell, therefore decoupling the fast-electron transport from the hydrodynamics. The Mo layer in all targets was ~30 $\mu$m thick, which absorbed most of the fast electrons. This prevented refluxing (the re-entry

E21989JR

Figure 135.22
Target geometries: (a) Mo-coated solid glass sphere was placed at the center of a nitrogen-filled CH shell. A series of targets with varying Mo outer diameters was used to study the divergence. (b) To extend the divergence measurements to a larger-diameter Mo shell, a Mo-coated CH shell target was used (overcoated with CH). (c) A photograph of a target of type (a) before being shot.

of fast electrons after reflection from the electrostatic sheath around the target) and isolated the effect of divergence. The space between the CH shell and the Mo ball was filled with $N_2$ at ~1 atm to minimize electric-field effects. The 60-beam OMEGA Laser System[17] was used for these experiments and was smoothed by distributed phase plates,[18] 2-D spectral dispersion,[19] and polarization rotators.[20]

The Mo–$K_\alpha$ line was measured by two identical planar LiF crystal spectrometers (XRS's), as well as a Cauchois-type quartz crystal spectrometer (TCS).[21] The high-energy continuum spectrum (HXR) was measured by the four-channel hard x-ray detector (HXRD) spectrometer[22] from which the fast-electron temperature was determined. The relative energy in x rays above ~50 keV, measured by one of these channels, is reported in this article.

Figure 135.23 shows the intensity of the Mo–$K_\alpha$ line measured by the XRS and TCS, as well as the HXR radiation measured by the HXRD spectrometer. The *EGSnrc* Monte Carlo (MC) code[23] was used to simulate the transport of fast electrons and the emission of the Mo $K_\alpha$ and the HXR; these results, assuming a wide divergence of the fast electrons, are
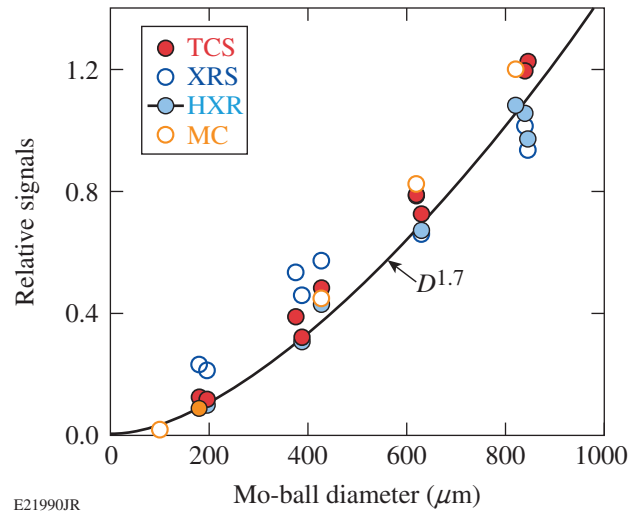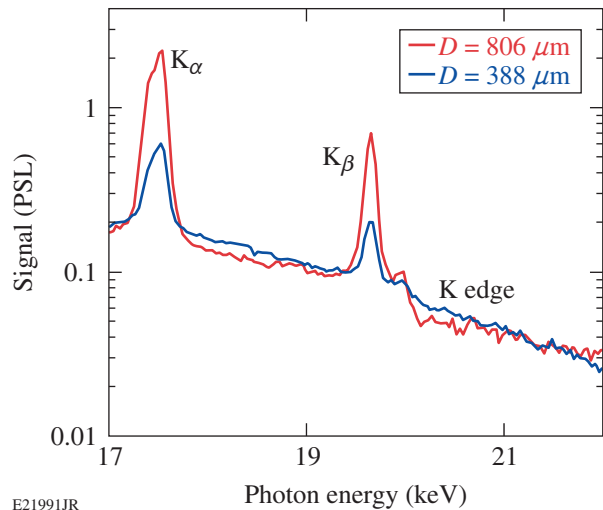


E21990JR

Figure 135.23
The intensity of the Mo–$K_\alpha$ line measured by the XRS and TCS, as well as the hard x-ray radiation measured by HXRD. The Monte Carlo (MC) simulation results for a divergent fast-electron beam are also shown. The curve is the best fit to the HXR data. The increase of the signals with the Mo-shell diameter indicates a wide-angle divergence of fast electrons.

shown in Fig. 135.23. The incident fast electrons in the simulations are assumed to start from a point on the outer surface of the target and move isotropically within a half space. Unlike the Mo–$K_\alpha$ line, hard x rays are also emitted by the outer CH shell (not just the Mo layer), but the emission from the CH is independent of the Mo diameter (see Fig. 135.24); therefore, it



E21991JR

Figure 135.24
The measured x-ray spectrum for two Mo-shell diameters, used to assess the pumping of the Mo–$K_\alpha$ line by continuum radiation (above the Mo K edge). The continuum is emitted mostly by the outer CH shell; therefore it is about the same for all Mo diameters. PSL: photostimulated luminescence.[24]

must be a fraction of the total HXR emission for the smallest-diameter Mo target. That fraction was determined by running the MC code for an empty CH shell and was then subtracted from the HXR signals of all targets. The spread of the points can be related to the high sensitivity of fast-electron production to the laser intensity. A ±1% variation in both the laser energy and the outer target diameter (±3% in the overlapped intensity) corresponds to about ±10% variation in the $K_\alpha$ and the HXR signals.[11] The curve is the best fit to the HXR data.

The results of Fig. 135.23 show that fast electrons have a divergence extending at least to the original target diameter. As explained above, this is the relevant measure in assessing fast-electron preheat in cryogenic direct-drive implosions. The x-ray signals are not exactly proportional to the area of the Mo ball. MC simulations show that for the largest-diameter Mo ball, electrons are significantly slowed down because they traverse the CH shell diagonally and are significantly scattered out of the Mo layer because of the large angle of incidence on that layer. Without these effects the signals for $D \sim 800\ \mu$m would align closer to a $D^2$ scaling. The most-obvious explanation for the close to $\sim D^2$ rise in Fig. 135.23 is the wide-angle divergence of the fast electrons. The exact shape of the rise is unimportant; the very fact that the curve rises is an indication of divergence since a radially directed electron beam would result in constant signals, independent of $D$. The indicated minimum fast-electron divergence is given by the solid angle of the largest Mo ball at a point on the quarter-critical layer. Three alternative explanations to the rise in signals were investigated: electron scattering in the outer CH shell, radiation excitation of the Mo–$K_\alpha$ line, and a radial electric field related to the return current within the ionized $N_2$ fill gas.

Electron scattering in the CH was shown to be relatively unimportant by MC simulations using a narrow (<1-$\mu$m) radial electron beam for various Mo diameters. For a non-scattered beam, the energy in the Mo–$K_\alpha$ line should be independent of $D$. Instead, the MC simulations showed that the energy rises with $D$ and reaches a plateau below $D \sim 300\ \mu$m. Scattering broadens the electron beam to an extent consistent with the early rise in Fig. 135.23 but not with the rest of the curve.

The $K_\alpha$ line is excited by fast electrons but could also be pumped by the plasma radiation from the laser absorption region in the CH. Unless this contribution is small, the rise of $K_\alpha$ yield with $D$ may not reflect fast-electron divergence (particularly since the radiation is isotropic). To examine this contribution to the measured $K_\alpha$ energy, the spectra for targets of two Mo diameters, $\sim 400$ and $\sim 800\ \mu$m, are shown

in Fig. 135.24. The ratio of the $K_\alpha$ line intensities for the two shots is, as expected, about equal to the ratio in areas of the Mo balls. The continuum, which is emitted by the outer CH shell, is about the same for the two targets. The radiation contribution to the $K_\alpha$ line can be calculated through the integral $E_R = \int I_c(E)\,\omega_K\big[(K_\alpha)/E\big]dE$, where $I_c(E)$ is the continuum spectrum, $\omega_K = 0.76$ is the $K_\alpha$ fluorescence yield of Mo, and the integral extends upward from the K edge (at $\sim 20$ keV). Only the relative intensity of the spectrum is required for calculating $E_R$. For the larger diameter, $E_R$ is less than $\sim 10\%$ of the total energy of the $K_\alpha$ line. For the smaller diameter, the relevant continuum intensity is smaller than that shown in Fig. 135.24 because the Mo shell intercepts only a fraction ($\sim 1/4$) of the CH continuum. The relative contribution of the radiation is the same for all Mo diameters (but can best be determined from the larger diameter). Therefore, radiation pumping of the Mo–$K_\alpha$ line is unimportant. Additionally, it should be emphasized that the HXR measurements, shown to track the $K_\alpha$ measurements in Fig. 135.23, are related only to the fast electrons, thereby confirming the conclusions on fast-electron divergence.

The rise in the signals with $D$ shown in Fig. 135.23 could be related to a retarding radial electric field caused by a return current that will reduce the values of the measured signals. For a radially directed fast-electron beam, the effect would increase with decreasing $D^2$ because of the increase in the fast-electron current density at decreasing radii. This possibility was addressed in two ways: First, the experiment was repeated using a lower laser energy (18 kJ instead of 26 kJ). This reduced the energy in fast electrons and consequently the electric field by a factor of $\sim 80$ (Ref. 11). Figure 135.25 shows the HXR signals for the two cases (the radiation contribution to the Mo–$K_\alpha$ line is larger for the low-power shots; therefore, the $K_\alpha$ data were omitted in Fig. 135.25). The shape of the two curves is approximately the same. If the rise in Fig. 135.23 resulted from electric-field effects, rather than fast-electron divergence, we would expect the lower-power curve to tend toward a constant value with increasing $D$.

Additionally, the electric field resulting from a return current in the $N_2$ gas between the Mo and CH shells has been estimated (no space charges can build up because they will lead to extremely high retarding fields). The total fast-electron current density at the quarter-critical surface was calculated as $J_{hot}(r_{1/4}) = f_{hot}eI_L/E_{hot}$, where $f_{hot}$ is the fraction of instantaneous laser power that is converted to fast-electron power, $I_L$ is the laser irradiance, and $E_{hot}$ is a typical fast-electron energy. For the shots reported in Fig. 135.23, $I_L = 1.1 \times 10^{15}$ W/cm$^2$ and the HXRD-measured hot-electron temperature is $\sim 50$ keV;
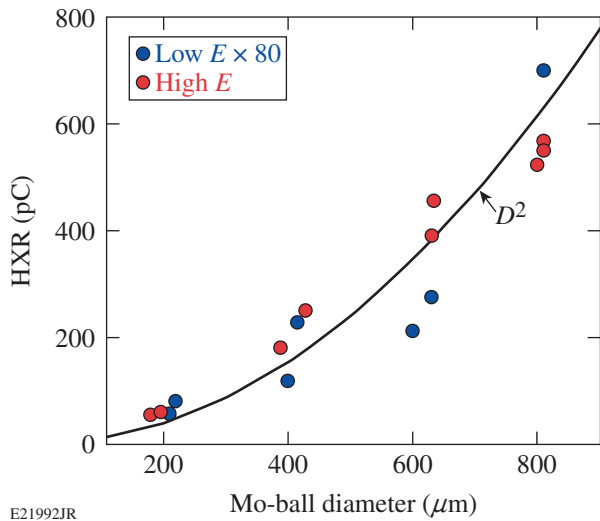
E21992JR

Figure 135.25
The hard x-ray measurements for 18- and 26-kJ laser energies, indicating a reduction by a factor ~80 in the production of fast electrons, consequently in the electric field. The $D^2$ curve serves merely to guide the eye. The similarity of the two sets of data sharply reduces the likelihood of electric-field effect on the results shown in Fig. 135.23.

(Refs. 11 and 12). Using Fig. 135.26(a), the instantaneous $f_{hot}$ was determined and used to calculate the time history of $J_{hot}(r_{1/4})$. The calculated total current is of the order of a few megaamperes, which is much above the Alfvén limiting current,[25] forcing a return current density equal to $J_{hot}(r)$. The return current gives rise to a resistive radial electric field given by $E(r) = J_{hot}(r)/\sigma(r)$, where $\sigma(r)$ is the parallel Braginskii conductivity:[26] $\sigma = 1.96\,Ne^2\tau_e/m_e$ in terms of the electron collision time $\tau_e$. We estimate $\sigma(r)$ using the temperature and ionization of the $N_2$ gas (no density dependence), simulated by the hydrodynamic code $LILAC$[27] for the case of a 200-$\mu$m-diam Mo ball. The fill gas was ionized by shock and radiation heating. Figure 135.26(b) shows the estimated electric potential drop across the $N_2$ gas for several times during the laser pulse. The time history of the field follows that of the HXR curve; the outer surface of the Mo layer is seen to expand in time as a result of heating by absorbed radiation; this is an additional source of ionization of the fill gas. The maximum electric potential is much smaller than typical fast-electron energy (~75 keV); therefore, the generated electric field has a negligible effect on the fast-electron current and the results shown in Fig. 135.23.

In conclusion, we have described a new technique for studying the divergence of fast electrons in laser fusion using Mo-coated balls embedded within CH shell targets. We have shown that the fast electrons generated on the OMEGA laser at an irradiance of ~1.1 × 10$^{15}$ W/cm$^2$ are widely divergent. This result greatly improves the outlook for direct-drive

therefore, for a three-dimensional Maxwellian distribution, $E_{hot} \sim 75$ keV. Figure 135.26(a) shows the time histories of the laser power and the HXR for one of the shots shown in Fig. 135.23. Note that most of the fast electrons are produced in the latter part of the laser pulse. For a laser irradiance of $1.1 \times 10^{15}$ W/cm$^2$, the time-integrated value of $f_{hot}$ is ~0.01
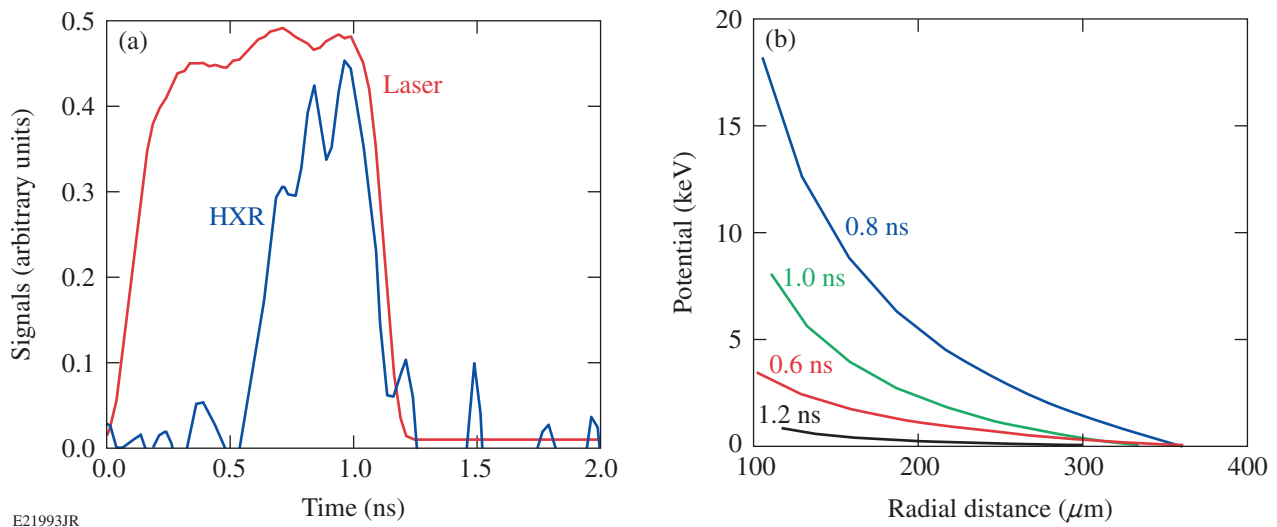


E21993JR

Figure 135.26
(a) The measured pulse shapes of the laser and hard x-ray (HXR) radiation. (b) The electric potential across the $N_2$ fill gas resulting from the return current produced by the radial fast-electron current is estimated at several times. The electric potential drop is much smaller than a typical fast-electron energy (~75 keV), thereby eliminating electric fields as a possible cause for the signal's rise shown in Fig. 135.23.

laser fusion by reducing the expected preheat. It also enables one to precisely determine the preheat in any given direct-drive laser-fusion experiment by using an electron-transport calculation in conjunction with a hydrodynamic code and a single observable: the emitted HXR. For imploding cryogenic targets on OMEGA, the maximum laser irradiance is $\sim 8 \times 10^{14}$ W/cm$^2$ and the total energy in fast electrons is $\sim 0.2\%$ of the laser energy,[11] but the results reported here show that only $\sim 1/4$ of the fast electrons will intersect the cold fuel and potentially preheat it. This reduces the fraction of fast-electron energy converted to preheat to less than $\sim 0.05\%$, well below the maximum tolerated. Therefore, preheat by fast electrons in current OMEGA cryogenic experiments is negligible. Polar-drive–ignition designs[28] for the National Ignition Facility (NIF)[29] with peak intensities of $1.1 \times 10^{15}$ W/cm$^2$ show[28] that the cold fuel shell has converged by about a factor 2 around the time of maximum density scale length; therefore, the same reduction in preheat caused by fast-electron divergence is expected for polar-drive–ignition experiments on the NIF.

## ACKNOWLEDGMENT

## REFERENCES

1. M. N. Rosenbluth, R. B. White, and C. S. Liu, Phys. Rev. Lett. **31**, 1190 (1973).

2. H. A. Baldis and C. J. Walsh, Phys. Fluids **26**, 1364 (1983).

3. B. B. Afeyan and E. A. Williams, Phys. Plasmas **4**, 3827 (1997).

4. C. Stoeckl, R. E. Bahr, B. Yaakobi, W. Seka, S. P. Regan, R. S. Craxton, J. A. Delettrez, R. W. Short, J. Myatt, A. V. Maximov, and H. Baldis, Phys. Rev. Lett. **90**, 235002 (2003).

5. J. D. Lindl, *Inertial Confinement Fusion: The Quest for Ignition and Energy Gain Using Indirect Drive* (Springer-Verlag, New York, 1998), Chap. 11.

6. *LLE Review Quarterly Report* **79**, 121, Laboratory for Laser Energetics, University of Rochester, Rochester, NY, LLE Document No. DOE/SF/19460-317, NTIS Order No. DE2002762802 (1999). Copies may be obtained from the National Technical Information Service, Springfield, VA 22161.

7. R. L. McCrory, D. D. Meyerhofer, R. Betti, R. S. Craxton, J. A. Delettrez, D. H. Edgell, V. Yu Glebov, V. N. Goncharov, D. R. Harding, D. W. Jacobs-Perkins, J. P. Knauer, F. J. Marshall, P. W. McKenty, P. B. Radha, S. P. Regan, T. C. Sangster, W. Seka, R. W. Short, S. Skupsky, V. A. Smalyuk, J. M. Soures, C. Stoeckl, B. Yaakobi, D. Shvarts, J. A. Frenje, C. K. Li, R. D. Petrasso, and F. H. Séguin, Phys. Plasmas **15**, 055503 (2008).

8. V. A. Smalyuk, D. Shvarts, R. Betti, J. A. Delettrez, D. H. Edgell, V. Yu. Glebov, V. N. Goncharov, R. L. McCrory, D. D. Meyerhofer, P. B. Radha, S. P. Regan, T. C. Sangster, W. Seka, S. Skupsky, C. Stoeckl, B. Yaakobi, J. A. Frenje, C. K. Li, R. D. Petrasso, and F. H. Séguin, Phys. Rev. Lett. **100**, 185005 (2008).

9. B. Yaakobi, P.-Y. Chang, A. A. Solodov, C. Stoeckl, D. H. Edgell, R. S. Craxton, S. X. Hu, J. F. Myatt, F. J. Marshall, W. Seka, and D. H. Froula, Phys. Plasmas **19**, 012704 (2012).

10. D. H. Froula, B. Yaakobi, S. X. Hu, P.-Y. Chang, R. S. Craxton, D. H. Edgell, R. Follett, D. T. Michel, J. F. Myatt, W. Seka, R. W. Short, A. Solodov, and C. Stoeckl, Phys. Rev. Lett. **108**, 165003 (2012).

11. D. H. Froula, D. T. Michel, I. V. Igumenshchev, S. X. Hu, B. Yaakobi, J. F. Myatt, D. H. Edgell, R. Follett, V. Yu. Glebov, V. N. Goncharov, T. J. Kessler, A. V. Maximov, P. B. Radha, T. C. Sangster, W. Seka, R. W. Short, A. A. Solodov, C. Sorce, and C. Stoeckl, Plasma Phys. Control. Fusion **54**, 124016 (2012).

12. D. T. Michel, A. V. Maximov, R. W. Short, J. A. Delettrez, D. Edgell, S. X. Hu, I. V. Igumenshchev, J. F. Myatt, A. A. Solodov, C. Stoeckl, B. Yaakobi, and D. H. Froula, Phys. Plasmas **20**, 055703 (2013).

13. V. N. Goncharov, T. C. Sangster, T. R. Boehly, S. X. Hu, I. V. Igumenshchev, F. J. Marshall, R. L. McCrory, D. D. Meyerhofer, P. B. Radha, W. Seka, S. Skupsky, C. Stoeckl, D. T. Casey, J. A. Frenje, and R. D. Petrasso, Phys. Rev. Lett. **104**, 165001 (2010).

14. S. P. Regan, N. B. Meezan, L. J. Suter, D. J. Strozzi, W. L. Kruer, D. Meeker, S. H. Glenzer, W. Seka, C. Stoeckl, V. Yu. Glebov, T. C. Sangster, D. D. Meyerhofer, R. L. McCrory, E. A. Williams, O. S. Jones, D. A. Callahan, M. D. Rosen, O. L. Landen, C. Sorce, and B. J. MacGowan, Phys. Plasmas **17**, 020703 (2010).

15. B. Yaakobi, T. R. Boehly, T. C. Sangster, D. D. Meyerhofer, B. A. Remington, P. G. Allen, S. M. Pollaine, H. E. Lorenzana, K. T. Lorenz, and J. A. Hawreliak, Phys. Plasmas **15**, 062703 (2008).

16. T. Döppner *et al.*, Phys. Rev. Lett. **108**, 135006 (2012).

17. T. R. Boehly, D. L. Brown, R. S. Craxton, R. L. Keck, J. P. Knauer, J. H. Kelly, T. J. Kessler, S. A. Kumpan, S. J. Loucks, S. A. Letzring, F. J. Marshall, R. L. McCrory, S. F. B. Morse, W. Seka, J. M. Soures, and C. P. Verdon, Opt. Commun. **133**, 495 (1997).

18. Y. Lin, T. J. Kessler, and G. N. Lawrence, Opt. Lett. **20**, 764 (1995).

19. S. Skupsky, R. W. Short, T. Kessler, R. S. Craxton, S. Letzring, and J. M. Soures, J. Appl. Phys. **66**, 3456 (1989).

20. T. R. Boehly, V. A. Smalyuk, D. D. Meyerhofer, J. P. Knauer, D. K. Bradley, R. S. Craxton, M. J. Guardalben, S. Skupsky, and T. J. Kessler, J. Appl. Phys. **85**, 3444 (1999).

21. J. F. Seely *et al.*, Rev. Sci. Instrum. **81**, 10E301 (2010).

22. C. Stoeckl, V. Yu. Glebov, D. D. Meyerhofer, W. Seka, B. Yaakobi, R. P. J. Town, and J. D. Zuegel, Rev. Sci. Instrum. **72**, 1197 (2001).

23. I. Kawrakow *et al.*, NRC, Ottawa, Canada, NRCC Report PIRS-701 (May 2011); I. Kawrakow, Med. Phys. **27**, 485 (2000).

24. A. L. Meadowcroft, C. D. Bentley, and E. N. Stott, Rev. Sci. Instrum. **79**, 113102 (2008).

25. S. Atzeni and J. Meyer-ter-Vehn, *The Physics of Inertial Fusion: Beam Plasma Interaction, Hydrodynamics, Hot Dense Matter*, International Series of Monographs on Physics (Clarendon Press, Oxford, 2004), p. 423.

26. S. I. Braginskii, in *Reviews of Plasma Physics*, edited by Acad. M. A. Leontovich (Consultants Bureau, New York, 1965), Vol. 1, p. 205.

27. R. Epstein, S. Skupsky, and J. Delettrez, J. Quant. Spectrosc. Radiat. Transf. **35**, 131 (1986).

28. T. J. B. Collins, J. A. Marozas, K. S. Anderson, R. Betti, R. S. Craxton, J. A. Delettrez, V. N. Goncharov, D. R. Harding, F. J. Marshall, R. L. McCrory, D. D. Meyerhofer, P. W. McKenty, P. B. Radha, A. Shvydky, S. Skupsky, and J. D. Zuegel, Phys. Plasmas **19**, 056308 (2012).

29. G. H. Miller, E. I. Moses, and C. R. Wuest, Opt. Eng. **43**, 2841 (2004).